Selectivity and Mass Transfer Limitations in Pressure-Retarded Osmosis at High Concentrations and Increased Operating Pressures

4 AUTHORS, INCLUDING:

Anthony P. Straub
Yale University
11 PUBLICATIONS **164** CITATIONS

SEE PROFILE

Tzahi Cath
Colorado School of Mines
81 PUBLICATIONS **3,202** CITATIONS

SEE PROFILE

Menachem Elimelech
Yale University
395 PUBLICATIONS **32,649** CITATIONS

SEE PROFILE

Selectivity and Mass Transfer Limitations in Pressure-Retarded Osmosis at High Concentrations and Increased Operating Pressures

Anthony P. Straub,[†] Chinedum O. Osuji,[†] Tzahi Y. Cath,[‡] and Menachem Elimelech[*,†]

[†]Department of Chemical and Environmental Engineering, Yale University, New Haven, Connecticut 06520-8286, United States
[‡]Department of Civil and Environmental Engineering, Colorado School of Mines, Golden, Colorado 80401-1887, United States

S *Supporting Information*

ABSTRACT: Pressure-retarded osmosis (PRO) is a promising source of renewable energy when hypersaline brines and other high concentration solutions are used. However, membrane performance under conditions suitable for these solutions is poorly understood. In this work, we use a new method to characterize membranes under a variety of pressures and concentrations, including hydraulic pressures up to 48.3 bar and concentrations of up to 3 M NaCl. We find membrane selectivity decreases as the draw solution concentration is increased, with the salt permeability coefficient increasing by a factor of 2 when the draw concentration is changed from 0.6 to 3 M NaCl, even when the applied hydraulic pressure is maintained constant. Additionally, we find that significant pumping energy is required to overcome frictional pressure losses in the spacer-filled feed channel and achieve suitable mass transfer on the feed side of the membrane, especially at high operating pressures. For a meter-long module operating at 41 bar, we estimate feedwater will have to be pumped in at a pressure of at least 3 bar. Both the reduced selectivity and increased pumping energy requirements we observe in PRO will significantly diminish the obtainable net energy, highlighting important new challenges for development of systems utilizing hypersaline draw solutions.
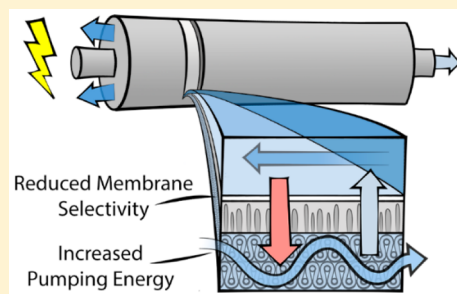
INTRODUCTION

Anthropogenic climate change has motivated a rapid increase in research activity to shift the global energy production portfolio away from fossil fuels.[1] A promising and currently untapped renewable source is the energy released upon mixing two solutions of different concentrations, commonly referred to as salinity gradient energy.[2,3] Several technologies have been developed to extract salinity gradient energy, including pressure-retarded osmosis (PRO),[4,5] reverse electrodialysis,[6,7] capacitive mixing,[8,9] and hydrogel swelling.[10] Of these technologies, PRO is one of the most widely researched and has been demonstrated at the pilot scale.[5,11−13] Recent comparisons to similar technologies have shown that PRO has greater potential in terms of both efficiency and cost.[14,15]

The PRO process employs a semipermeable membrane between a low concentration feed solution and a high concentration draw solution. Water molecules, driven by osmosis, diffuse through the membrane from the feed to the draw solution. The expanding volume of the draw solution is restricted, causing a hydraulic pressure buildup. The diluted draw solution is then depressurized through a hydroturbine to generate electricity

PRO is typically considered for extracting the energy available where rivers meet the sea.[16,17] However, recent work modeling full-scale systems has shown that the energy extractable from this solution pairing may not be sufficient to overcome the energetic costs of pretreatment and pumping.[18,19] Instead, higher concentration gradients with a greater energy extractable per unit of solution volume may be necessary to generate a substantial net energy. Higher concentration draw solutions are available from a variety of systems: natural sources including hypersaline water bodies[20] or subsurface reservoirs;[21] anthropogenic waste streams, such as brines from seawater desalination;[22−24] and engineered solutions, which can be employed in an osmotic heat engine to extract useful energy from low-grade heat sources.[25,26]

Effective operation with higher concentration draw solutions requires increased hydraulic pressure differences across the membrane since both the power density and the efficiency of energy extraction are maximized when the applied hydraulic pressure is equal to approximately half the osmotic pressure difference between the draw and feed solution.[18,19] The performance of the system is therefore constrained by the physical integrity of the membrane module. In small-scale experiments, few membranes have been tested at pressures appropriate for high concentration draw solutions, with only one example, from our prior work, of operation at pressures greater than 24 bar.[27]

Since relatively few tests have been conducted at higher pressures and concentrations, the effect of these operating conditions on overall system performance is uncertain.

Accurate knowledge of intrinsic membrane properties during operation is critical to realistically model system efficiency and understand design factors for membranes.[19,28,29] Most studies on PRO, even those at lower pressures, have only focused on a comparison of basic performance metrics, such as water flux or power density, between different membranes.[30−34] Of the studies that also measured the reverse salt flux during PRO operation, a significant discrepancy was observed between the experimental measurements in pressurized operation and predictions based on membrane properties determined in reverse osmosis (RO).[35−38] These observations strongly indicate that membrane properties may be altered during PRO operation.

In this study, we examine intrinsic membrane properties in high pressure PRO using concentrated draw solutions. To understand how membrane properties are affected by these conditions, we present a new method to determine membrane transport and structural parameters using both water flux and reverse salt flux measurements during PRO operation. Draw solution concentration and hydraulic pressure are systematically varied to obtain membrane properties under a wide range of conditions, including high hydraulic pressures (up to 48 bar) and increased concentrations (up to 3 M NaCl) rarely tested in the literature. We also examine the trade-off between frictional pressure loss in the feed channel and mass transfer on the feed side of the membrane, a crucial consideration for the net energy output of a PRO system. Finally, we discuss implications of our analysis for the design and promise of PRO with high concentration gradients.

■ MATERIALS AND METHODS

PRO Membrane, Spacers, and Experimental Setup. Commercial flat-sheet, thin-film composite (TFC) forward osmosis (FO) membranes from Hydration Technology Innovations (Albany, OR) were used in all experiments. Our previous work demonstrated that these membranes can operate at pressures up to 48 bar, in part due to their robust polysulfone support layer reinforced by an embedded polyester mesh.[27] Membranes were loaded into a crossflow test cell and oriented with the active layer facing the concentrated draw solution and the support layer facing the feed solution.

Experiments were conducted in a custom-made bench-scale experimental PRO setup described previously.[27] In the membrane test cell, both channels were 10.7 cm long and 3.6 cm wide, with only a 9.9 cm by 3.4 cm portion of the membrane exposed. The draw channel height was approximately 1 mm. Unless otherwise noted, the draw solution flow rate was kept constant at 0.8 L min^{-1}, and the feed solution flow rate was maintained at 0.04 L min^{-1}. Temperature was measured near the flow cell outlets using thermocouples and maintained at 25 ± 0.5 °C.

Feed channel spacers placed between the membrane support layer and the feed channel wall served to support the membrane under pressure and maintain channel geometry. Only woven fabrics were selected for the feed channel spacers as preliminary testing showed that coarser plastic spacers caused the membranes to severely deform and rupture at low pressures. Three different types of fabric were employed as feed channel spacers that fell into the general categories of a fine, medium, and coarse weave. Two layers of a given fabric type were used in each experiment, except in the case of the coarse spacer, which exhibited rupture at lower pressures and thus required a layer of the medium spacer to be placed between the

coarse spacer and the membrane. The thickness of the spacer determined the channel height on the feed side of the membrane, with an approximate channel height of 0.45, 0.5, and 0.7 mm for the fine, medium, and coarse spacers, respectively. In the draw channel, a biplanar extruded netting spacer was employed to enhance mixing.

Determination of Membrane Transport and Structural Properties During PRO Operation. The intrinsic water permeability coefficient, A, NaCl permeability coefficient, B, and structural parameter of the support layer, S, were determined in a single experiment. The membranes were first compacted for at least 10 h at the applied hydraulic pressure, ΔP, intended for the experiment while circulating deionized (DI) water on both sides of the membrane. After compaction, the stable DI water flux, J_w^{DI}, was recorded. The water permeability coefficient, A, was calculated by dividing the water flux by the corresponding applied pressure, $A = J_w^{DI}/\Delta P$.[39]

After measuring the DI water flux, the concentration in the draw solution reservoir was increased to 50 mM NaCl. In this scenario, ΔP is much higher than the osmotic pressure difference across the membrane, $\Delta \pi$, and water continues to permeate from the draw reservoir to the feed reservoir (i.e., negative PRO flux). Stable water and salt flux measurements with the 50 mM NaCl solution in the draw channel were used to calculate the mass transfer coefficient on the draw side of the membrane, k, and verify the integrity of the membrane, as described in the Supporting Information.

Measurements in PRO operation with a high concentration draw solution (0.6−3 M NaCl) were then used to determine the NaCl permeability coefficient, B, and the effective structural parameter, S_{eff}. After the addition of salt to the draw solution and flux reversal, the water flux (J_w), salt flux (J_s), bulk feed concentration ($c_{F,b}$), and bulk draw concentration ($c_{D,b}$) were measured. The experimental measurements, along with the previously determined A and k values, were used to calculate the B and S_{eff} values as well as the feed concentration at the active layer surface ($c_{F,m}$), the draw concentration at the active layer surface ($c_{D,m}$), the feed osmotic pressure at the active layer surface ($\pi_{F,m}$), and the draw osmotic pressure at the active layer surface ($\pi_{D,m}$) using the following equations:[40]

$$J_w = A(\pi_{D,m} - \pi_{F,m} - \Delta P) \tag{1}$$

$$J_s = B(c_{D,m} - c_{F,m}) \tag{2}$$

$$c_{D,m} = c_{D,b} \exp\left(-\frac{J_w}{k}\right) - \frac{B}{J_w}(c_{D,m} - c_{F,m})\left[1 - \exp\left(-\frac{J_w}{k}\right)\right] \tag{3}$$

$$c_{F,m} = c_{F,b} \exp\left(\frac{J_w S_{eff}}{D}\right) + \frac{B}{J_w}(c_{D,m} - c_{F,m})\left[\exp\left(\frac{J_w S_{eff}}{D}\right) - 1\right] \tag{4}$$

where D is the NaCl diffusion coefficient, and the osmotic pressure, π, is related to the concentration, c, using the following relationship determined with OLI Stream Analyzer:

$$\pi = A_1 c + A_2 c^2 + A_3 c^3$$
$$(A_1 = 44.242, \ A_2 = 4.5690, \ A_3 = 0.55332) \tag{5}$$

For experiments where membrane properties were measured at multiple applied hydraulic pressures, the membrane was first compacted at the highest operating pressure. With DI water still circulating on both sides, the pressure was then incrementally
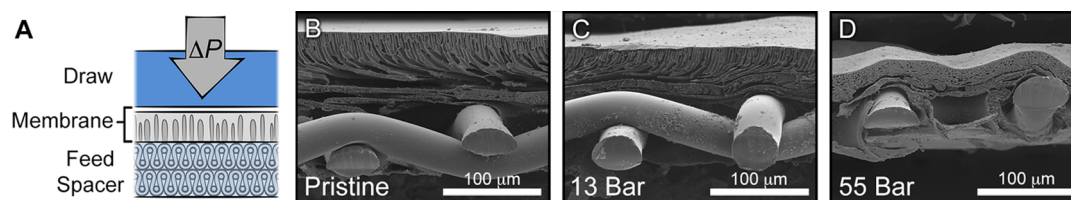
Figure 1. (A) Schematic diagram of the PRO membrane and spacer during operation. SEM micrographs of HTI thin-film composite (TFC) membrane cross sections for (B) a pristine membrane sample, (C) a membrane after compaction at an applied hydraulic pressure of 13 bar, and (D) a membrane after compaction at 55 bar.

decreased, and the stable water flux was recorded at each step to determine the water permeability, A. Subsequently, the pressure was increased back to the initial compaction pressure, and the stable DI water flux was measured to verify membrane properties had not changed. Measurements with a 50 mM NaCl solution in the draw reservoir were then used to determine the draw side mass transfer coefficient, k, before the draw concentration was further increased to the desired concentration for PRO operation. Another incremental decrease in pressure was performed to measure the water and salt flux in PRO at each pressure. From these measurements, the B and S_{eff} values were determined at each pressure. Prior to conducting experiments, we verified that pressure cycling did not detrimentally affect membrane properties for three cycles with ΔP varied from 0 to 30 bar.

The effective structural parameter term, S_{eff}, in this study represents the same mass transfer resistances on the feed side of the membrane as in many past studies.[5,34,41−43] As in previous work, it is not truly a representation of structural properties of the membrane *per se*, since all feed side mass transfer resistances are inevitably lumped into this term.[44] These resistances include effects from both internal concentration polarization in the porous support and additional external concentration polarization on the support side of the membrane.[45−47] Experimentally distinguishing between different mass transfer resistances on the support side of the membrane in experiments has proven difficult, since even internal concentration polarization can change based on differences in mixing at the membrane support surface.[44] Nevertheless, the use of the lumped effective structural parameter allows for facile comparison of our results with previous work, and the term can be easily related to an effective feed side mass transfer coefficient, $k_{F,eff} = D/S_{eff}$.

The characterization method introduced in this study distinguishes itself from previous methods by using both water flux and reverse salt flux measurements during PRO operation to calculate the membrane parameters at a specific operating pressure.[16,22,48,49] It also relates osmotic pressure to molar concentration using a nonlinear relationship, which is necessary at higher concentrations that deviate significantly from the commonly used van't Hoff equation. However, there are still underlying assumptions in the calculation method. Specifically, we assume tight, salt-rejecting membranes; the mass transfer coefficient on the draw side of the membrane, k, is assumed to be constant for a given experiment regardless of the applied hydraulic pressure or flux across the membrane; and the NaCl diffusion coefficient is assumed constant with a value of 1.48×10^{-9} m^2/s.[50]

Feed Channel Pressure Loss Experiments. Experiments were conducted to measure pressure loss across the feed channel, ΔP_F, and effective structural parameter, S_{eff}, with the three different spacer types and varying crossflow velocities.

After the membrane and spacer were loaded into the cell and compacted, A and k were determined as discussed previously. The draw solution concentration was then increased to the desired concentration (1 M NaCl for ΔP of 13 bar and 2 M NaCl for ΔP of 41 bar). After flux reversal, the crossflow velocity in the feed channel was varied, and ΔP_F was measured at each velocity using a pressure gauge mounted at the feed channel inlet. In a manner analogous to the previous subsection, S_{eff} was calculated at each crossflow velocity.

Characterization of Membranes in RO and FO Operation. For comparison, membrane properties were determined using two additional established techniques. In the first technique, henceforth referred to as the RO and FO characterization, the active layer properties were determined from water flux and salt rejection measurements in an RO test cell, and the structural parameter was calculated using a water flux measurement from FO operation. An applied hydraulic pressure of 24 bar and a 50 mM NaCl feed solution were used for RO tests, and a 1 M NaCl draw solution was used for FO water flux tests. The RO and FO characterization represents one of the most widely used techniques to determine the properties of a given FO membrane, and a detailed protocol is available in the literature.[41]

Membrane properties were also determined without any applied hydraulic pressure using only measurements in FO and a fitting algorithm. This FO-only characterization method is extensively described elsewhere.[51]

■ RESULTS AND DISCUSSION

Membrane and Spacer Properties Determine Performance in PRO. The high hydraulic pressures used in pressure-retarded osmosis (PRO) and the requirement for membrane thickness to be minimized to aid in mass transfer[52] create a scenario where thin membranes are compacted strongly against the feed spacer (Figure 1A). The overall performance of the PRO system will therefore be determined by the membrane materials and structure, which may deform significantly as the pressure is increased, as well as the properties of the underlying spacer on which the membrane rests.[35,48] Optimization of both components in the system is necessary to maximize system performance, especially at high operating pressures that impart a significant amount of strain on the membrane.

SEM micrographs of membrane cross sections after operation at different hydraulic pressures, presented in Figure 1, give qualitative insights into the possible effects of pressurized operation on membrane performance. A pristine membrane cross section is shown (Figure 1B) alongside membrane cross sections after operation at 13 bar (Figure 1C) and 55 bar (Figure 1D). The 13 bar applied hydraulic pressure represents the optimal condition for mixing river water and

seawater,[19] while 55 bar is representative of a hydraulic pressure appropriate for hypersaline draw solutions.

From the images in Figure 1, we identify multiple changes in membrane structure that may affect performance. For the pristine membrane, the membrane compacted at 13 bar, and the membrane compacted at 55 bar, the total membrane thickness is 145 μm, 120 μm, and 85 μm, respectively. The dramatic decrease in support layer thickness as pressure increases is evidently a result of the support layer pore structure collapsing on top of the underlying spacer. Alterations to the thickness, porosity, and tortuosity of the support layer after compaction will inevitably affect mass transfer within the support layer.[53] Additionally, deformation of the active layer during high pressure operation may also impact water and salt permeability or concentration polarization on the draw side of the membrane. Transport behavior of membrane support and active layers will be thoroughly analyzed in the following subsections.

Small Spacer Pore Sizes Allow for Increased Operating Pressures. The spacer used in the feed channel for PRO is a critical design consideration.[35,48] An optimal feed spacer must simultaneously support the membrane under high hydraulic pressures, allow for suitable mass transfer in the feed channel, and minimize frictional losses as water flows through the module. We evaluated three different types of feed spacers for their suitability in PRO. Spacers could be distinguished by their structure and opening size (Figure 2A) and fall into the categories of a fine, medium, and coarse weave with opening sizes of approximately 170, 350, and 550 μm, respectively.
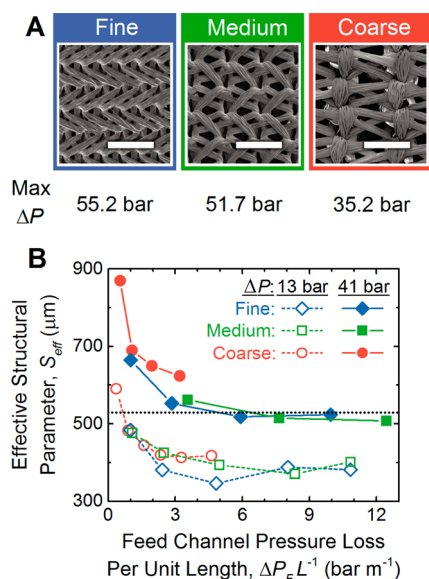

Figure 2. (A) SEM micrographs of the three fabric feed spacers tested in this study and their respective maximum operating pressures (Max ΔP). The scale bar is 1 mm. (B) Effective structural parameter, S_{eff}, vs feed channel pressure loss per unit length, $\Delta P_F/L$, for two layers of each spacer type, with the exception of the coarse spacer, which rested below a medium spacer to enable operation at higher pressures. Tests were conducted at applied hydraulic pressure differences across the membrane, ΔP, of 13 bar (hollow symbols and dashed lines) and 41 bar (solid symbols and lines). Draw solutions of 1 M NaCl and 2 M NaCl were used for the 13 and 41 bar experiments, respectively, with a DI water feed. The dotted black line indicates the structural parameter measured with no applied pressure and no spacer.

Initial tests were conducted to determine the maximum operating pressure a membrane placed on each type of spacer was able to withstand before rupturing. Here, rupture was indicated by a rapid, more than 3-fold increase in the water flux across the membrane in the direction of the hydraulic pressure driving force. The same type of commercial membrane was used in all experiments. We observed a monotonic increase of maximum operating pressure with smaller opening sizes of the spacer woven fabric (Figure 2A). The coarse, medium, and fine spacers demonstrated maximum operating pressures of 35.2, 51.7, and 55.2 bar, respectively.

The Trade-off between Feed Channel Pressure Loss and Concentration Polarization Is Exacerbated at Higher Pressures. The three different spacers were employed during the evaluation of concentration polarization on the feed side of the membrane and frictional pressure losses in the feed channel. Two parameters were used to describe performance effects. The *feed channel pressure loss per unit length*, $\Delta P_F/L$, is defined as the loss in hydraulic pressure along the feed channel normalized by the channel length. Minimizing the feed channel pressure loss in PRO is crucial, as the pumping required to drive water flow through the narrow membrane channels can consume a significant amount of power and drastically reduce the net energy output of the process.

To describe mass transfer on the feed side of the membrane, the *effective structural parameter*, S_{eff}, is used. This term is widely employed to quantify internal concentration polarization caused by the membrane support layer,[5,34,41−43] although any additional mass transfer limitations in the feed channel will be inevitably combined in the term.[44] Reducing S_{eff} is imperative in PRO, as concentration polarization can severely reduce the water flux and overall performance of the system.

The crossflow velocity in the feed channel was systematically varied during PRO operation, and measurements at each crossflow velocity were used to calculate $\Delta P_F/L$ and S_{eff}. When comparing S_{eff} to $\Delta P_F/L$ directly, all three spacers demonstrated a similar trade-off despite their varying structure and thickness (Figure 2B). As higher pressures are used to force water through the feed spacer (i.e., a higher $\Delta P_F/L$), the crossflow velocity in the feed channel also increases, leading to improved mass transfer on the feed side of the membrane. This observation is in line with previous work that also observed a decrease in the effective structural parameter at higher crossflow velocities[44,46] and indicates that mass transfer in the feed channel is dependent on system operating conditions. It is likely that the improvement in mass transfer as the crossflow velocity increases is due to a reduction in external concentration polarization outside of the support layer.[46]

When the applied hydraulic pressure in the system, ΔP, is increased from 13 to 41 bar, mass transfer on the feed side of the membrane suffers, as indicated by the increased S_{eff}. Even if the same crossflow velocity is used with a given spacer, mass transfer in the feed channel is hindered at higher pressures (complete set of data is shown in Figure S1 of the Supporting Information). This could be explained by detrimental changes in the membrane support structure after the high pressure deformation observed in Figure 1D occurs, resulting in a negatively impacted tortuosity or porosity. Additional mass transfer resistance may also occur outside the membrane as the porous support compacts strongly against the fabric feed spacer.

The observations shown here demonstrate that significant pumping pressure is needed to overcome frictional losses and
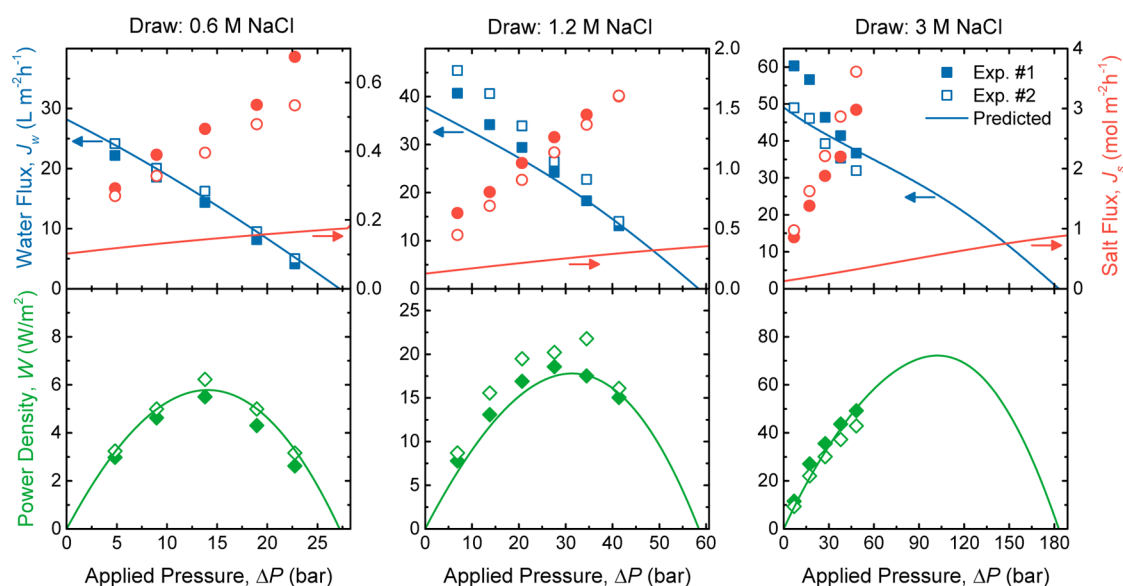
Figure 3. Complete set of water flux (blue squares), reverse salt flux (red circles), and power density (green diamonds) data for duplicate experimental runs with 0.6, 1.2, and 3 M NaCl draw solutions. Symbols represent experimental values, while lines show values predicted using eqs 1−4 and membrane properties determined in an RO and FO characterization (A = 1.77 L m^{-2} h^{-1} bar^{-1}, B = 0.30 L m^{-2} h^{-1}, and S = 702 μm). The 0.6, 1.2, and 3 M NaCl draw solutions correspond to osmotic pressures of 28.3, 60.6, and 188.8 bar, respectively, eq 5. All experiments were performed with feed (DI water) and draw solutions at 25 ± 0.5 °C.
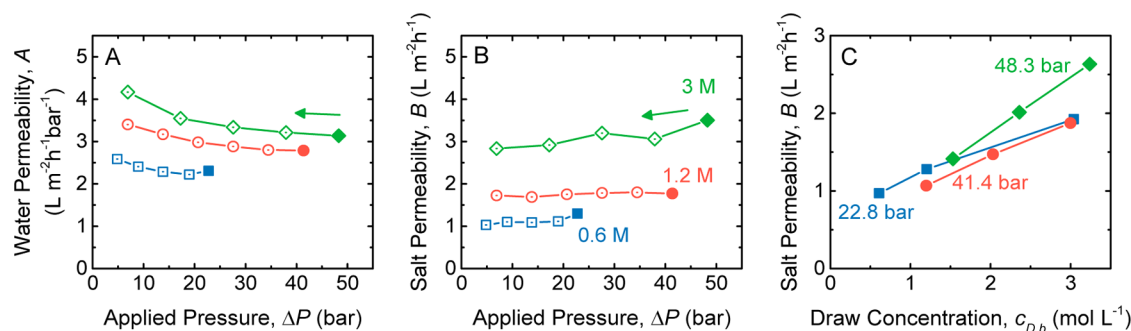

Figure 4. (A) Membrane water permeability coefficient, A, and (B) NaCl salt permeability coefficient, B, as a function of the hydraulic pressure difference, ΔP. The compaction pressure is indicated by solid points and pressure is incrementally decreased after compaction. All experiments were initially compacted at either 22.8 bar (blue squares), 41.4 bar (red circles), or 48.3 bar (green diamonds). In Figure 4B, draw solution concentrations of 0.6 M NaCl (blue), 1.2 M NaCl (red), and 3 M NaCl (green) are used. (C) Measured salt permeability coefficient as a function of the bulk draw concentration for three different compaction pressures: 22.8 bar (blue squares), 41.4 bar (red circles), and 48.3 bar (green diamonds). In all experiments, the feed is DI water.

generate flow along the feed channel. This pressure must be provided into the system for suitable mass transfer to occur on the feed side of the membrane. Pumping the feed solution represents an energy input to the system that should be minimized. However, if less energy is expended for pumping in the feed channel (i.e., the system is operated with a lower $\Delta P_F/L$), performance will suffer due to increased concentration polarization. Operating the system with a higher applied hydraulic difference across the membrane only worsens this effect, reducing mass transfer in the system or increasing the energy requirements for pumping. For a system operating at a ΔP of 41 bar to achieve an S_{eff} less than 550 μm, the feed solution would need to be pumped in at 3 bar per meter length of module, consuming a substantial amount of additional energy. For a module operating with a ΔP of 13 bar to achieve the same S_{eff} the feed solution would only need to be pumped at less than 1 bar per meter of module.

Measured Reverse Salt Fluxes are Substantially Higher than Predicted Values. The water flux and reverse

salt flux are useful to describe the performance of a membrane under a given set of conditions. We evaluated water flux and reverse salt flux in PRO with draw solution concentrations of 0.6, 1.2, and 3 M NaCl using the medium feed channel spacers discussed in the previous subsection. The 0.6 M NaCl draw solution is representative of seawater, the 1.2 M NaCl solution is equivalent to brine from a seawater RO desalination plant, and the 3 M NaCl draw solution is representative of a hypersaline brine. Each draw solution was tested with a DI water feed. The measured water and salt flux, as well as the calculated membrane power density, $W = J_w \Delta P$, are shown in Figure 3 (symbols) and compared to values predicted using membrane properties determined with a conventional RO and FO characterization method (A = 1.77 L m^{-2}h^{-1}bar^{-1}, B = 0.30 L m^{-2}h^{-1}, and S = 702 μm) and eqs 1−4 (lines).

For all three draw solution concentrations, the measured water fluxes and resultant power densities show reasonable agreement with predicted values. This agreement is seen even at the highest operating pressure tested (48.3 bar) and is in line

with results from our previous work demonstrating the feasibility of high power density PRO at increased hydraulic pressure.[27]

The experimental reverse salt fluxes in PRO were dramatically higher than predicted values. Even for the lowest compaction pressure (24 bar), where we would expect to see only minor deformation of the membrane, the experimental reverse salt fluxes are more than double the predicted values. At 48.3 bar with a 3 M NaCl draw solution, the experimental reverse salt flux is 10.2 times higher than the expected value. Other studies have reported similarly higher-than-expected reverse salt fluxes during PRO operation.[35−38]

Active Layer Properties are Affected by Operating Conditions. A characterization technique was developed that utilizes both water flux and reverse salt flux measurements from PRO operation to determine membrane properties at given pressure and draw concentration. This method differs from previous characterization methods, which did not use reverse salt flux measurements in PRO operation.[22,48,49] Figure 4 shows the active layer properties determined under a variety of conditions using the developed characterization technique.

The water permeability coefficient, A, at different hydraulic pressures is presented in Figure 4A. Three experimental runs are shown with different initial compaction pressures (solid symbol). Membranes with a higher compaction pressure demonstrated increased water permeabilities, an occurrence that is possibly attributed to permanent deformation of the membrane causing some stretching of the active layer—as was observed in SEM cross sections (Figure 1D). However, once the membrane was compacted, decreasing the pressure increased the water permeability. We suspect that the feed spacer may block portions of the membrane at higher pressures, a phenomenon that has been called the spacer shadow effect,[48] and this blockage may be relieved when the pressure is decreased. Nevertheless, the water permeability at the compaction pressure for all six experimental runs was consistently between 2 and 3 L m^{-2} h^{-1} bar^{-1} (Figure S2 in the Supporting Information).

The salt permeability of the membrane, B, at varying hydraulic pressure is shown in Figure 4B. Three fixed draw solution concentrations were used (0.6, 1.2, and 3 M NaCl) with different compaction pressures. For each of the three runs, we observe a slight decrease in the salt permeability coefficient as the applied hydraulic pressure is decreased from the initial compaction pressure. However, a much more dramatic change in the salt permeability is evident when comparing the values between different compaction pressures and draw solution concentrations. For the runs with a 0.6 M NaCl draw solution compacted at 22.8 bar (blue), a 1.2 M NaCl draw solution compacted at 41.4 bar (red), and a 3 M NaCl draw solution compacted at 48.3 bar (green), the salt permeabilities are 1.30, 1.77, and 3.50 L m^{-2} h^{-1}, respectively.

In an attempt to decouple the effect of compaction pressure and draw solution concentration, we conducted three experiments with membranes compacted at a fixed pressure (22.8, 41.4, or 48.3 bar), and while holding all other parameters constant, we incrementally increased the draw solution concentration (Figure 4C). We observe a strong dependence of B on the draw concentration for all compaction pressures, indicating that it is the increase in concentration—not the higher operating pressure—which is responsible for a majority of the increased salt permeability observed in Figure 4B. For example, at a compaction pressure of 22.8 bar, the salt

permeability increases from 0.97 L m^{-2} h^{-1} to 1.93 L m^{-2} h^{-1} when the draw concentration is changed from 0.6 to 3 M NaCl. The increase in salt permeability at higher concentrations disagrees with the common assumption that solute sorption and diffusivity through the polyamide active layer are relatively independent of solution composition.[39,54] Additional experiments and possible explanations for this phenomenon will be presented later in the discussion.

During each experiment, the mass transfer coefficient on the draw side of the membrane, k, was determined (Figure S3). Generally, the draw side mass transfer coefficient tended to increase as the applied hydraulic pressure increased. This may be a result of the membrane active layer deforming around the supporting mesh, as shown in Figure 1, and inducing more mixing at the membrane surface.

Membrane Salt Permeability Is Dependent on Interface Salt Concentration. In the previous subsection, we observed an increase in the salt permeability coefficient as the bulk draw salt concentration was increased. If the selectivity of the membrane is affected by solution composition, it is the concentration at the active layer interface, not the bulk concentration, that will affect transport. Using the characterization results from PRO operation and eqs 1−4, we can determine these interface concentrations for a variety of different bulk compositions and applied hydraulic pressures. Similarly, the interface salt concentration in FO and RO characterizations can also be determined. The resulting data set allows for the comparison of salt permeability coefficients as a function of the average active layer interface concentration for a wide range of operating pressures, flux directions, and bulk salt compositions (Figure 5). For each experiment, the average active layer interface concentration is simply determined as the
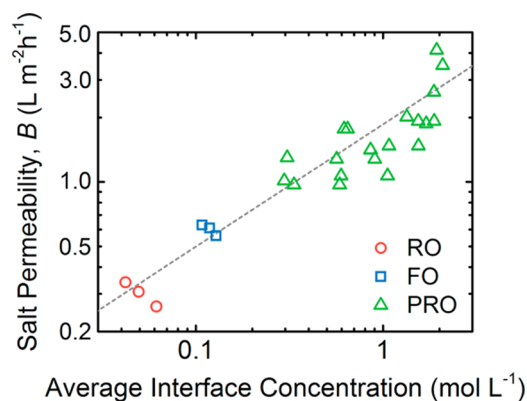

Figure 5. Log−log plot of the salt permeability coefficient, B, as a function of the average membrane interface NaCl concentration. For each measurement, the average interface concentration is determined as the mean of the concentrations calculated on either side of the membrane active layer accounting for concentration polarization. Results from three different operational modes are shown. Reverse osmosis (RO) tests were conducted with an applied pressure of 24.1 bar and a feed concentration of 50 mM NaCl. Forward osmosis (FO) experiments were conducted with varying draw concentrations, a DI water feed, and no applied hydraulic pressure. Pressure-retarded osmosis (PRO) tests were conducted at applied hydraulic pressures ranging from 22.8 to 48.3 bar and draw NaCl concentrations ranging from 0.6 to 3 M. Temperature maintained at 25 ± 0.5 °C for all experiments. To guide the eye, a monomial fit in the form $y = ax^n$ is included where $a = 1.86$ and $n = 0.572$ ($R^2 = 0.92$).

mean of the concentrations calculated on either side of the membrane active layer.

The data shown in Figure 5 clearly indicates the salt permeability coefficient of the membrane increases at higher interface salt concentrations; this trend is observed for measurements taken in the FO, RO, and PRO modes and is not discernably affected by operating pressures ranging from 0 to 48 bar. The salt permeability coefficient determined in RO at a hydraulic pressure of 24.1 bar was lower than in FO testing conducted with no hydraulic pressure. PRO testing, which was conducted at varying pressures from 22.8 to 48.3 bar, showed a range of salt permeability coefficients depending on the concentration at the active layer interface. We note that the trend is consistent even though distinct characterization techniques were used for each operating mode; more details on experimental procedures and calculations are given in the Supporting Information.

The concentration effects observed in this study are highly relevant to PRO, since the high concentration draw solution is placed directly in contact with the active layer. In FO, high draw solution concentrations can also be used, but dilution will occur due to internal concentration polarization in the membrane support layer.[55] In RO, the feed concentration is limited because the osmotic pressure cannot exceed the applied hydraulic pressure driving water across the membrane.[56]

Donnan Exclusion and Decreased Hydrated Ion Radii May Explain Reduced Selectivity. The above results indicate that the salt permeability coefficient of the membrane is strongly dependent on the salt concentration the active layer is in contact with. This finding challenges the conventional solution-diffusion equation used to determine salt flux eq 2, where the salt permeability is assumed to remain constant irrespective of operating conditions. While it is beyond the scope of this study to rigorously investigate the many possible mechanisms of increased salt passage, we postulate possible reasons for the unexpected selectivity behavior that warrant further investigation.

The observations in this study may be due to Donnan exclusion effects in the membrane active layer. Polyamide membranes have abundant carboxyl groups that will partly dissociate in the relevant pH range (6.5−8.0); this dissociation causes polyamide to behave as a weakly charged polymer.[57] As with any charged polymer, at low concentrations, the sorption and diffusion of co-ions are hindered by electrostatic repulsion in a phenomenon known as Donnan exclusion.[58,59] In the case of sodium chloride transport, slowed diffusion of chloride ions—which bear the same charge as the deprotonated carboxyl groups—will also reduce the transport of sodium, since charge neutrality across the membrane must be maintained. As the salt concentration increases, ion−polymer interactions are increasingly screened, and salt sorption into and diffusivity through the charged polymer layer will increase.[58] Donnan exclusion effects have been observed in thin-film composite membranes for FO,[60] and increases in salt permeability with ionic strength have also been observed in RO using polyamide membranes.[61] It is possible that the high salt concentrations in this study lead to similar charge screening effects, and the apparent power law relation of salt permeability with interface concentration in Figure 5 is similar to that expected from charged polymeric materials.[62]

Another possible explanation for the increased salt permeability is that the effective size of salts diffusing through the polyamide layer decreases at higher concentrations. The diffusivity of ions through polyamide is highly dependent on their hydrated size.[62] At higher concentrations, the hydrated radius of ions can decrease,[63] and increases in concentration also result in ion pairing, which may also increase diffusivity.[64,65] When the salts are dissolved in the polymer matrix, these effects can be exacerbated as compared to in bulk solution. However, it is very challenging to experimentally probe ion hydration and pairing behavior in hydrated polymers, making this effect difficult to validate.[62]

It is also possible that transport across the membrane occurs through a combination of solution-diffusion through the dense polymer active layer and pore flow through defects in the membrane. A theory for this behavior was initially developed by Sherwood to describe performance in RO[66] and has been used recently to explain measurements in pressure-assisted FO.[67] However, the lack of a substantial salt permeability dependence on pressure in our results renders this explanation improbable, and preliminary attempts to describe our observations through a similar model were unsuccessful.

Implications for Process Performance. This study has identified critical challenges to PRO performance with high concentration draw solutions and increased hydraulic pressure. Specifically, we find that to achieve adequate mass transfer on the feed side of the membrane at high hydraulic pressures, substantial pumping energy must be expended. Additionally, we observe a significant decrease in membrane selectivity when operating with increased draw concentrations, leading to greatly exacerbated reverse salt leakage across the membrane.

The increased salt permeability observed at high concentrations defies the common assumption that solute diffusivity and sorption in polyamide membranes are independent of draw concentration and has implications for all osmotic membrane processes using highly saline solutions. For our coupon-scale PRO experiments, the reduced selectivity does not significantly affect the water flux or power density. However, increased reverse salt flux will substantially reduce the efficiency and power density of a full-scale PRO system[19,38] and may also lead to regions within the module where flux is reversed.[19] Therefore, the higher-than-expected reverse salt flux must be further understood and mitigated, or a substantial portion of the energy gained from using higher concentration gradients in PRO may be lost.

The trade-off identified between feed channel pressure loss and mass transfer will also result in a substantially reduced system efficiency. Our experiments indicate that for membrane modules operating at 41 bar, influent water will have to be pumped in at an applied pressure of at least 3 bar per meter length of module in order for appropriate mass transfer on the feed side of the membrane to be achieved. Since the energy that can be extracted from a PRO system is equal to the applied hydraulic pressure multiplied by the transmembrane flow rate, and the transmembrane flow rate is always less than the feed flow rate, it is straightforward to estimate the minimum efficiency loss due to pumping. For example, a meter-long module operating at 41 bar would expend at least 7% of the gross extracted energy on pumping feed solutions at 3 bar.

We previously conducted a theoretical analysis on the extractable energy and efficiency of realistic PRO systems.[18,19] From this analysis, we identified the energy extractable from river water mixing with seawater is relatively low and may not be sufficient to overcome energetic costs associated with operation. We concluded that higher concentration alternative draw solutions, like reverse osmosis desalination concentrate

streams or hypersaline brines, might offer significantly greater extractable energies. In this work, we have revealed new challenges for PRO operation with high concentration draw solutions and find that interpreting membrane properties as constant regardless of the operating conditions is not a valid assumption. However, we also demonstrate water fluxes and power densities that are substantial, even under extreme conditions, highlighting the promise of using higher concentration solution pairings in pressure-retarded osmosis. By further improving our understanding of membrane performance, developing innovative fabrication methods, and utilizing inventive membrane modules, engineers and scientists may continue to drive PRO technology toward higher concentration solution pairings and greater extractable energy.

■ ASSOCIATED CONTENT

ⓈSupporting Information

The Supporting Information is available free of charge on the ACS Publications website at DOI: 10.1021/acs.est.5b01317.

> Details on the methodology for determining the draw mass transfer coefficient, k, and verifying membrane selectivity during a PRO experiment; procedures for calculating the concentration at the active layer interface in FO and RO; full list of membrane parameters determined in FO and RO operation (Table S1); data on the effective structural parameter and feed channel pressure loss as a function of crossflow velocity (Figure S1); the complete set of calculated active layer properties during pressure cycling (Figure S2); and the draw side mass transfer coefficient, k, determined during PRO testing (Figure S3) (PDF)

■ AUTHOR INFORMATION

Corresponding Author

*Phone: +1 (203) 432-2789. Fax: +1 (203) 432-2881. E-mail: menachem.elimelech@yale.edu.

Notes

The authors declare no competing financial interest.

■ ACKNOWLEDGMENTS

■ REFERENCES

(1) Hoffert, M. I.; Caldeira, K.; Benford, G.; Criswell, D. R.; Green, C.; Herzog, H.; Jain, A. K.; Kheshgi, H. S.; Lackner, K. S.; Lewis, J. S.; et al. Advanced Technology Paths to Global Climate Stability: Energy for a Greenhouse Planet. *Science* **2002**, *298*, 981−987.

(2) Logan, B. E.; Elimelech, M. Membrane-Based Processes for Sustainable Power Generation Using Water. *Nature* **2012**, *488*, 313−319.

(3) Pattle, R. E. Production of Electric Power by Mixing Fresh and Salt Water in the Hydroelectric Pile. *Nature* **1954**, *174*, 660.

(4) Loeb, S. Osmotic Power Plants. *Science* **1975**, *189*, 654−655.

(5) Helfer, F.; Lemckert, C.; Anissimov, Y. G. Osmotic Power with Pressure Retarded Osmosis: Theory, Performance and Trends − A Review. *J. Membr. Sci.* **2014**, *453*, 337−358.

(6) Yip, N. Y.; Vermaas, D. a; Nijmeijer, K.; Elimelech, M. Thermodynamic, Energy Efficiency, and Power Density Analysis of Reverse Electrodialysis Power Generation with Natural Salinity Gradients. *Environ. Sci. Technol.* **2014**, *48*, 4925−4936.

(7) Daniilidis, A.; Vermaas, D. a.; Herber, R.; Nijmeijer, K. Experimentally Obtainable Energy from Mixing River Water, Seawater or Brines with Reverse Electrodialysis. *Renewable Energy* **2014**, *64*, 123−131.

(8) Hatzell, M. C.; Cusick, R. D.; Logan, B. E. Capacitive Mixing Power Production from Salinity Gradient Energy Enhanced through Exoelectrogen-Generated Ionic Currents. *Energy Environ. Sci.* **2014**, *7*, 1159−1165.

(9) Rica, R.; Ziano, R.; Salerno, D.; Mantegazza, F.; van Roij, R.; Brogioli, D. Capacitive Mixing for Harvesting the Free Energy of Solutions at Different Concentrations. *Entropy* **2013**, *15*, 1388−1407.

(10) Zhu, X.; Yang, W.; Hatzell, M. C.; Logan, B. E. Energy Recovery from Solutions with Different Salinities Based on Swelling and Shrinking of Hydrogels. *Environ. Sci. Technol.* **2014**, *48*, 7157−7163.

(11) Achilli, A.; Childress, A. E. Pressure Retarded Osmosis: From the Vision of Sidney Loeb to the First Prototype Installation — Review. *Desalination* **2010**, *261*, 205−211.

(12) Skilhagen, S. E. Osmotic Power — a New, Renewable Energy Source. *Desalin. Water Treat.* **2010**, *15*, 271−278.

(13) Kurihara, M.; Hanakawa, M. Mega-Ton Water System: Japanese National Research and Development Project on Seawater Desalination and Wastewater Reclamation. *Desalination* **2013**, *308*, 131−137.

(14) Ramon, G. Z.; Feinberg, B. J.; Hoek, E. M. V. Membrane-Based Production of Salinity-Gradient Power. *Energy Environ. Sci.* **2011**, *4*, 4423−4434.

(15) Yip, N. Y.; Elimelech, M. Comparison of Energy Efficiency and Power Density in Pressure Retarded Osmosis and Reverse Electrodialysis. *Environ. Sci. Technol.* **2014**, *48*, 11002−11012.

(16) Thorsen, T.; Holt, T. The Potential for Power Production from Salinity Gradients by Pressure Retarded Osmosis. *J. Membr. Sci.* **2009**, *335*, 103−110.

(17) Maisonneuve, J.; Pillay, P.; Laflamme, C. B. Osmotic Power Potential in Remote Regions of Quebec. *Renewable Energy* **2015**, *81*, 62−70.

(18) Lin, S.; Straub, A. P.; Elimelech, M. Thermodynamic Limits of Extractable Energy by Pressure Retarded Osmosis. *Energy Environ. Sci.* **2014**, *7*, 2706−2714.

(19) Straub, A. P.; Lin, S.; Elimelech, M. Module Scale Analysis of Pressure Retarded Osmosis: Performance Limitations and Implications for Full-Scale Operation. *Environ. Sci. Technol.* **2014**, *48*, 12435−12444.

(20) Loeb, S. Energy Production at the Dead Sea by Pressure-Retarded Osmosis: Challenge or Chimera? *Desalination* **1998**, *120*, 247−262.

(21) Wick, G.; Isaacs, J. Salt Domes: Is There More Energy Available from Their Salt than from Their Oil? *Science* **1978**, *199*, 1436−1437.

(22) Achilli, A.; Prante, J. L.; Hancock, N. T.; Maxwell, E. B.; Childress, A. E. Experimental Results from RO-PRO: A next Generation System for Low-Energy Desalination. *Environ. Sci. Technol.* **2014**, *48*, 6437−6443.

(23) Altaee, A.; Sharif, A.; Zaragoza, G.; Ismail, A. F. Evaluation of FO-RO and PRO-RO Designs for Power Generation and Seawater Desalination Using Impaired Water Feeds. *Desalination* **2015**, *368*, 27−35.

(24) Kim, J.; Park, M.; Snyder, S. A.; Kim, J. H. Reverse Osmosis (RO) and Pressure Retarded Osmosis (PRO) Hybrid Processes: Model-Based Scenario Study. *Desalination* **2013**, *322*, 121−130.

(25) McGinnis, R. L.; McCutcheon, J. R.; Elimelech, M. A Novel Ammonia−Carbon Dioxide Osmotic Heat Engine for Power Generation. *J. Membr. Sci.* **2007**, *305*, 13−19.

(26) Lin, S.; Yip, N. Y.; Cath, T. Y.; Osuji, C. O.; Elimelech, M. Hybrid Pressure Retarded Osmosis - Membrane Distillation System for Power Generation from Low-Grade Heat: Thermodynamic Analysis and Energy Efficiency. *Environ. Sci. Technol.* **2014**, *48*, 5306−5313.

(27) Straub, A.; Yip, N.; Elimelech, M. Raising the Bar: Increased Hydraulic Pressure Allows Unprecedented High Power Densities in Pressure-Retarded Osmosis. *Environ. Sci. Technol. Lett.* **2014**, *1*, 55−59.

(28) Banchik, L. D.; Sharqawy, M. H.; Lienhard, J. H. Limits of Power Production due to Finite Membrane Area in Pressure Retarded Osmosis. *J. Membr. Sci.* **2014**, *468*, 81−89.

(29) Feinberg, B. J.; Ramon, G. Z.; Hoek, E. M. V. Scale-up Characteristics of Membrane-Based Salinity-Gradient Power Production. *J. Membr. Sci.* **2015**, *476*, 311−320.

(30) Achilli, A.; Cath, T. Y.; Childress, A. E. Power Generation with Pressure Retarded Osmosis: An Experimental and Theoretical Investigation. *J. Membr. Sci.* **2009**, *343*, 42−52.

(31) Chou, S.; Wang, R.; Shi, L.; She, Q.; Tang, C.; Fane, A. G. Thin-Film Composite Hollow Fiber Membranes for Pressure Retarded Osmosis (PRO) Process with High Power Density. *J. Membr. Sci.* **2012**, *389*, 25−33.

(32) Song, X.; Liu, Z.; Sun, D. D. Energy Recovery from Concentrated Seawater Brine by Thin-Film Nanofiber Composite Pressure Retarded Osmosis Membranes with High Power Density. *Energy Environ. Sci.* **2013**, *6*, 1199−1210.

(33) Han, G.; Zhang, S.; Li, X.; Chung, T. S. High Performance Thin Film Composite Pressure Retarded Osmosis (PRO) Membranes for Renewable Salinity-Gradient Energy Generation. *J. Membr. Sci.* **2013**, *440*, 108−121.

(34) Chou, S.; Wang, R.; Fane, A. G. Robust and High Performance Hollow Fiber Membranes for Energy Harvesting from Salinity Gradients by Pressure Retarded Osmosis. *J. Membr. Sci.* **2013**, *448*, 44−54.

(35) She, Q.; Hou, D.; Liu, J.; Tan, K. H.; Tang, C. Y. Effect of Feed Spacer Induced Membrane Deformation on the Performance of Pressure Retarded Osmosis (PRO): Implications for PRO Process Operation. *J. Membr. Sci.* **2013**, *445*, 170−182.

(36) Bui, N.; McCutcheon, J. Nanofiber Supported Thin-Film Composite Membrane for Pressure-Retarded Osmosis. *Environ. Sci. Technol.* **2014**, *48*, 4129−4136.

(37) She, Q.; Jin, X.; Tang, C. Y. Osmotic Power Production from Salinity Gradient Resource by Pressure Retarded Osmosis: Effects of Operating Conditions and Reverse Solute Diffusion. *J. Membr. Sci.* **2012**, *401*, 262−273.

(38) Zhang, S.; Chung, T. S. Minimizing the Instant and Accumulative Effects of Salt Permeability to Sustain Ultrahigh Osmotic Power Density. *Environ. Sci. Technol.* **2013**, *47*, 10085−10092.

(39) Baker, R. W. *Membrane Technology and Applications*, 2nd ed.; J. Wiley: New York, 2004.

(40) Yip, N. Y.; Tiraferri, A.; Phillip, W. A.; Schiffman, J. D.; Hoover, L. A.; Kim, Y. C.; Elimelech, M. Thin-Film Composite Pressure Retarded Osmosis Membranes for Sustainable Power Generation from Salinity Gradients. *Environ. Sci. Technol.* **2011**, *45*, 4360−4369.

(41) Yip, N. Y.; Tiraferri, A.; Phillip, W. A.; Schiffman, J. D.; Elimelech, M. High Performance Thin-Film Composite Forward Osmosis Membrane. *Environ. Sci. Technol.* **2010**, *44*, 3812−3818.

(42) Bui, N.; McCutcheon, J. R. Hydrophilic Nanofibers as New Supports for Thin Film Composite Membranes for Engineered Osmosis. *Environ. Sci. Technol.* **2013**, *47*, 1761−1769.

(43) Han, G.; Wang, P.; Chung, T. S. Highly Robust Thin-Film Composite Pressure Retarded Osmosis (PRO) Hollow Fiber Membranes with High Power Densities for Renewable Salinity-Gradient Energy Generation. *Environ. Sci. Technol.* **2013**, *47*, 8070−8077.

(44) Bui, N.-N.; Arena, J. T.; McCutcheon, J. R. Proper Accounting of Mass Transfer Resistances in Forward Osmosis: Improving the Accuracy of Model Predictions of Structural Parameter. *J. Membr. Sci.* **2015**, *492*, 289−302.

(45) Nagy, E. A General, Resistance-in-Series, Salt- and Water Flux Models for Forward Osmosis and Pressure-Retarded Osmosis for Energy Generation. *J. Membr. Sci.* **2014**, *460*, 71−81.

(46) Gruber, M. F.; Johnson, C. J.; Tang, C. Y.; Jensen, M. H.; Yde, L.; Hélix-Nielsen, C. Computational Fluid Dynamics Simulations of Flow and Concentration Polarization in Forward Osmosis Membrane Systems. *J. Membr. Sci.* **2011**, *379*, 488−495.

(47) Sivertsen, E.; Holt, T.; Thelin, W. R.; Brekke, G. Iso-Watt Diagrams for Evaluation of Membrane Performance in Pressure Retarded Osmosis. *J. Membr. Sci.* **2015**, *489*, 299−307.

(48) Kim, Y. C.; Elimelech, M. Adverse Impact of Feed Channel Spacers on the Performance of Pressure Retarded Osmosis. *Environ. Sci. Technol.* **2012**, *46*, 4673−4681.

(49) Kim, Y. C.; Kim, Y.; Oh, D.; Lee, K. H. Experimental Investigation of a Spiral-Wound Pressure-Retarded Osmosis Membrane Module for Osmotic Power Generation. *Environ. Sci. Technol.* **2013**, *47*, 2966−2973.

(50) Vitagliano, V.; Lyons, P. A. Diffusion Coefficients for Aqueous Solutions of Sodium Chloride and Barium Chloride. *J. Am. Chem. Soc.* **1956**, *78*, 1549−1552.

(51) Tiraferri, A.; Yip, N. Y.; Straub, A. P.; Romero-Vargas Castrillón, S.; Elimelech, M. A Method for the Simultaneous Determination of Transport and Structural Parameters of Forward Osmosis Membranes. *J. Membr. Sci.* **2013**, *444*, 523−538.

(52) Lee, K.; Baker, R.; Lonsdale, H. Membranes for Power Generation By Pressure-Retarded Osmosis. *J. Membr. Sci.* **1981**, *8*, 141−171.

(53) Tiraferri, A.; Yip, N. Y.; Phillip, W. A.; Schiffman, J. D.; Elimelech, M. Relating Performance of Thin-Film Composite Forward Osmosis Membranes to Support Layer Formation and Structure. *J. Membr. Sci.* **2011**, *367*, 340−352.

(54) Wijmans, J. G.; Baker, R. W. The Solution-Diffusion Model: A Review. *J. Membr. Sci.* **1995**, *107*, 1−21.

(55) McCutcheon, J. R.; Elimelech, M. Influence of Concentrative and Dilutive Internal Concentration Polarization on Flux Behavior in Forward Osmosis. *J. Membr. Sci.* **2006**, *284*, 237−247.

(56) Deshmukh, A.; Yip, N. Y.; Lin, S.; Elimelech, M. Desalination by Forward Osmosis: Identifying Performance Limiting Parameters through Module-Scale Modeling. *J. Membr. Sci.* **2015**, *491*, 159−167.

(57) Tiraferri, A.; Elimelech, M. Direct Quantification of Negatively Charged Functional Groups on Membrane Surfaces. *J. Membr. Sci.* **2012**, *389*, 499−508.

(58) Geise, G. M.; Freeman, B. D.; Paul, D. R. Sodium Chloride Diffusion in Sulfonated Polymers for Membrane Applications. *J. Membr. Sci.* **2013**, *427*, 186−196.

(59) Geise, G. M.; Falcon, L. P.; Freeman, B. D.; Paul, D. R. Sodium Chloride Sorption in Sulfonated Polymers for Membrane Applications. *J. Membr. Sci.* **2012**, *423–424*, 195−208.

(60) Lu, X.; Boo, C.; Elimelech, M. Bidirectional Diffusion of Ammonium and Sodium Cations in Forward Osmosis: Role of Membrane Active Layer Surface Chemistry and Charge. *Environ. Sci. Technol.* **2014**, *48*, 14369−14376.

(61) Bason, S.; Oren, Y.; Freger, V. Ion Transport in the Polyamide Layer of RO Membranes: Composite Membranes and Free-Standing Films. *J. Membr. Sci.* **2011**, *367*, 119−126.

(62) Geise, G. M.; Paul, D. R.; Freeman, B. D. Fundamental Water and Salt Transport Properties of Polymeric Materials. *Prog. Polym. Sci.* **2014**, *39*, 1−42.

(63) Afanas'ev, V. N. Solvation of Electrolytes and Nonelectrolytes in Aqueous Solutions. *J. Phys. Chem. B* **2011**, *115*, 6541−6563.

(64) Lyubartsev, A. P.; Laaksonen, A. Concentration Effects in Aqueous NaCl Solutions. A Molecular Dynamics Simulation. *J. Phys. Chem.* **1996**, *100*, 16410−16418.

(65) Marcus, Y.; Hefter, G. Ion Pairing. *Chem. Rev.* **2006**, *106*, 4585−4621.

(66) Sherwood, T.; Brian, P.; Fisher, R. Desalination by Reverse Osmosis. *Ind. Eng. Chem. Fundam.* **1967**, *6*, 2−12.

(67) Duan, J.; Litwiller, E.; Pinnau, I. Solution-Diffusion with Defects Model for Pressure-Assisted Forward Osmosis. *J. Membr. Sci.* **2014**, *470*, 323−333.